

Micro-Grid Simulation during Grid-Connected and Islanded Modes of Operation

F. D. Kanellos, A. I. Tsouchnikas, N. D. Hatziaargyriou, *Senior Member, IEEE*

Abstract—Technology evolution, environmental concerns associated with central electric power plants and deregulation of the electric utility industry are providing the opportunity for small distributed generators to become very important in order to satisfy the on – site customer expanding power demand.

In this paper, the steady state and transient operation of a typical microgrid are studied. The models of two dispersed generation units (photovoltaic system, wind turbine) are presented. Models of the power electronics interface and control strategies for fast control of frequency and voltage magnitude without communication are derived.

Keywords: microgrids, modeling, dispersed generation, wind turbine, photovoltaic system, control, islanding, power electronics interface.

I. INTRODUCTION

MICROGRIDS comprise low voltage distribution systems with distributed energy resources, such as photovoltaic power systems and wind turbines, together with storage devices. These systems are interconnected to the medium voltage distribution network, but they can be also operated isolated from the main grid.

From the customer point of view, microgrids provide both thermal and electricity needs and in addition enhance local reliability, reduce emissions, improve power quality by supporting voltage and reducing voltage dips and potentially lower costs of energy supply. From the utility point of view, application of distributed energy sources can potentially reduce the demand for distribution and transmission facilities. Clearly, distributed generation located close to loads will reduce flows in transmission and distribution circuits with two important effects: loss reduction and ability to potentially substitute for network assets. Furthermore, the presence of generation close to demand could increase service quality seen

by end customers. Microgrids can provide network support in times of stress by relieving congestions and aiding restoration after faults.

The development of microgrids can contribute to the reduction of emissions and the mitigation of climate changes. This is because available and currently developing technologies for distributed generation units are based on renewable sources and micro sources that are characterized by very low emissions.

Technical challenges associated with the operation and control of microgrids are immense. Ensuring stable operation during network disturbances, maintaining stability and power quality in the islanding mode of operation requires the development of sophisticated control strategies for microgrid's inverters in order to provide stable frequency and voltage in the presence of arbitrarily varying loads. This paper's objectives are to demonstrate the transients of a microgrid due to intentional islanding process and to illustrate the maintenance of stability of the microgrid in the isolated mode of operation for varying loads and climate conditions.

The control approach used in this paper is the implementation of conventional f/P , V/Q droops into the grid-side inverter, thus downscaling the conventional grid control concept to the BES inverter. In this way, expensive control bus systems requiring communication and extra cabling are avoided. Furthermore, for the adjustment of the frequency, the output active power of the inverter is measured and the output frequency is estimated according to the frequency droop. This approach presents several advantages as low cost, simple expansion of the system, increased redundancy and simplified supervisory control [1].

II. MICROGRID SYSTEM COMPONENTS AND MODELING

A single line diagram of the microgrid system studied in this paper is illustrated in Fig. 1. The microsources considered comprise a photovoltaic generator equipped with a Maximum Power Point Tracker (MPPT) and a fixed speed wind turbine equipped with an induction generator. A battery is used as energy storage unit and is simply represented as a DC voltage source with adequate capacity, capable of meeting the real and reactive power commands within pre-specified limits.

The authors would like to express their thanks to the European Commission for their support in the *MicroGrids*- project ENK5-CT-2002-00610.

F. D. Kanellos is with the School of Electrical and Computer Engineering, National Technical University of Athens, Greece (e-mail: kanellos@mail.ntua.gr).

A. I. Tsouchnikas is with the School of Electrical and Computer Engineering, National Technical University of Athens, Greece (e-mail: aggelos@power.ece.ntua.gr).

N. D. Hatziaargyriou is with the School of Electrical and Computer Engineering, National Technical University of Athens, Greece (e-mail: nh@power.ece.ntua.gr).

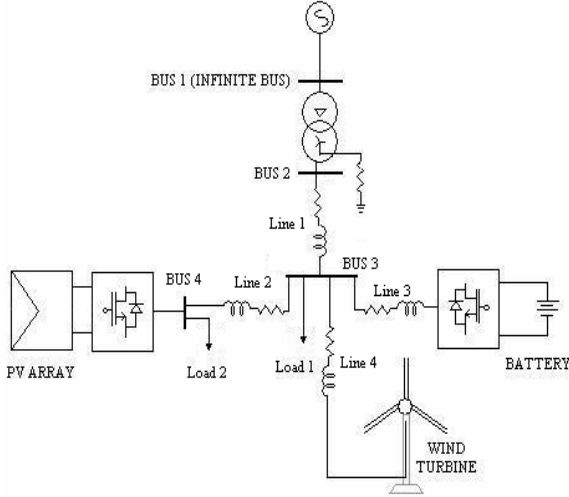


Fig. 1. Single-line diagram of the examined microgrid

A. Fixed Speed Wind Turbine Equipped with Induction Generator

For the modeling of the wind turbine rotor aerodynamics, the well – known aerodynamic power coefficient method $C_p(\lambda)$ is used:

$$P_a = \omega_r \cdot T_w = \frac{1}{2} \cdot \rho \cdot A \cdot C_p(\lambda, \beta) \cdot V_w^3 \quad (1)$$

where P_a is the aerodynamic power, $C_p(\lambda)$ is the dimensionless aerodynamic power performance coefficient, λ is the tip speed ratio, $\rho = 1.25 \text{ kg/m}^3$ is the air density, $A = \pi R^2$ is the rotor swept area, V_w is the wind speed, ω_r is the blade rotating speed and T_w the aerodynamic torque.

The equivalent of three elastically connected masses is used for simulating the mechanical system of the wind turbine (Fig. 2). The state space equations of the mechanical system are the following [2]:

$$\frac{d}{dt} \begin{bmatrix} \theta \\ \omega \end{bmatrix} = \begin{bmatrix} [0]_{3 \times 3} & [I]_{3 \times 3} \\ -\frac{1}{2} [H]^{-1} [C] & -\frac{1}{2} [H]^{-1} [D] \end{bmatrix} \begin{bmatrix} \theta \\ \omega \end{bmatrix} + \begin{bmatrix} [0]_{3 \times 3} \\ \frac{1}{2} [H]^{-1} \mathbf{T} \end{bmatrix} \quad (2)$$

where $\theta^T = [\theta_r, \theta_{gb}, \theta_g]$ is the angular position vector, $\omega^T = [\omega_r, \omega_{gb}, \omega_g]$ is the angular speed vector and $\mathbf{T}^T = [T_w, 0, T_g]$ is the external torque vector comprising the aerodynamic and the electromagnetic torque, T_w and T_g acting on the turbine and generator rotor, respectively.

$H = \begin{bmatrix} H_r & 0 & 0 \\ 0 & H_{gb} & 0 \\ 0 & 0 & H_g \end{bmatrix}$ is the inertia matrix,

$[C] = \begin{bmatrix} C_{HGB} & -C_{HGB} & 0 \\ -C_{HGB} & C_{HGB} + C_{GBG} & -C_{GBG} \\ 0 & -C_{GBG} & C_{GBG} \end{bmatrix}$ is the stiffness matrix,

$[D] = \begin{bmatrix} D_r + d_{HGB} & -d_{HGB} & 0 \\ -d_{HGB} & D_{GB} + d_{HGB} + d_{GBG} & -d_{GBG} \\ 0 & -d_{GBG} & D_g + d_{GBG} \end{bmatrix}$ is the

damping matrix, $[0]_{3 \times 3}$ is the zero 3x3 matrix and $[I]_{3 \times 3}$ is the identical 3x3 matrix. C matrix represents the low and high-speed shaft elasticities while D represents the internal friction and the torque losses. Subscripts $\{r\}$, $\{gb\}$ and $\{g\}$ denote turbine rotor, gear-box and generator, respectively.

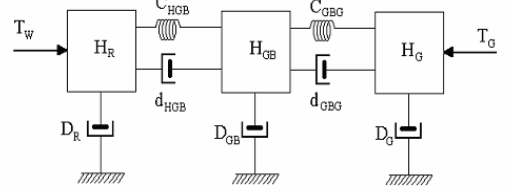


Fig. 2. Three masses drive train mechanical equivalent

For the induction generator, the well – known 4th order dq model is used, expressed in the arbitrary reference frame, rotating with an angular velocity ω [3]:

$$u_{sd} = -r_s \cdot i_{sd} - \omega \cdot \Psi_{sq} + p \Psi_{sd}$$

$$u_{sq} = -r_s \cdot i_{sq} + \omega \cdot \Psi_{sd} + p \Psi_{sq} \quad (3)$$

$$u_{rd} = 0 = r_r \cdot i_{rd} - (\omega - \omega_r) \cdot \Psi_{rq} + p \Psi_{rd}$$

$$u_{rq} = 0 = r_r \cdot i_{rq} + (\omega - \omega_r) \cdot \Psi_{rd} + p \Psi_{rq}$$

where $p = \frac{1}{\omega_o} \frac{d}{dt}$, and ω_o is the base electrical angular

frequency. Generator convention is used for the stator currents. The zero sequence equation is omitted, since the machine stator is Δ connected. The stator and rotor fluxes are related to the currents by:

$$\Psi_{sd} = -X_s \cdot i_{sd} + X_m \cdot i_{rd}$$

$$\Psi_{sq} = -X_s \cdot i_{sq} + X_m \cdot i_{rq} \quad (4)$$

$$\Psi_{rd} = -X_m \cdot i_{sd} + X_r \cdot i_{rd}$$

$$\Psi_{rq} = -X_m \cdot i_{sq} + X_r \cdot i_{rq}$$

The electromagnetic torque is given by:

$$T_e = \Psi_{qr} \cdot i_{dr} - \Psi_{dr} \cdot i_{qr} \quad (5)$$

The wind turbine implemented in this paper is stall controlled and directly connected to the low voltage grid with no power electronics interface [2,4].

B. Photovoltaic Array with MPP Tracker

The building block of a PV array is the solar cell, which is basically a p-n semiconductor junction that directly converts light energy into electricity. A solar cell is usually represented by an electrical equivalent one-diode model [5]-[8], as shown in Fig. 3:

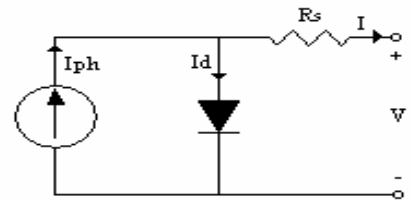


Fig. 3. Equivalent model for a single solar cell

The current source I_{ph} represents the cell photocurrent and R_s is the series resistance of the cell. PV cells are grouped in larger units called PV modules, which are further interconnected in a parallel-series configuration to form PV arrays or PV generators. For an array with N_s series connected cells and N_p parallel-connected cells, the array current may be related to the array voltage as [5]:

$$I = N_p [I_{ph} - I_{rs} [\exp(\frac{q(V + IR_s)}{AKTN_s}) - 1]] \quad (6)$$

where

$$I_{rs} = I_{rr} (\frac{T}{T_r})^3 \exp[\frac{E_G}{AK} (\frac{1}{T_r} - \frac{1}{T})] \quad (7)$$

and q is the charge of an electron, K is Boltzmann's constant, A is the diode ideality factor, T is the cell temperature (K), I_{rs} is the cell reverse saturation current at T , T_r is the cell reference temperature, I_{rr} is the reverse saturation current at T_r and E_G is the band gap energy of the semiconductor used in the cell. The photocurrent I_{ph} depends on the cell's temperature and radiation as follows:

$$I_{ph} = [I_{SCR} + k_i(T - T_r)] \frac{S}{100} \quad (8)$$

Where, I_{SCR} is the cell short circuit current at reference temperature and radiation, k_i is the short circuit current temperature coefficient and S is the solar radiation in mW/cm^2 . The power-voltage characteristic of the simulated PV array is shown in Fig. 4 (at reference temperature $T_r = 28.18^\circ\text{C}$).

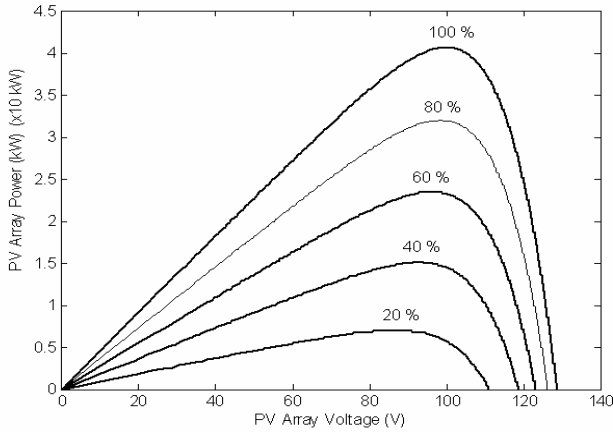


Fig. 4. Power-Voltage Simulated Characteristic of the PV Array

The maximum power point tracking technique used was the incremental conductance method. The basic idea is that at the Maximum Power Operating Point (MPOP) the derivative of the power with respect to the voltage vanishes because the MPOP is the maximum of the power curve, as shown in Fig. 4. Note that to the left of the MPOP the power is increasing with the voltage, i.e. $dP/dV > 0$ and it is decreasing to the right of the MPOP, i.e. $dP/dV < 0$. Hence, at the MPOP:

$$dP/dV = 0 \Rightarrow V dI/dV + I = 0 \Rightarrow dI/dV = -I/V \quad (9)$$

Measuring the incremental and instantaneous array conductance, the PV array voltage can be adjusted to the MPOP voltage [9,10].

C. PV Array Inverter Control System

The control system of the inverter of the PV array [11,12] consists of two major control loops: the reactive power and the DC voltage control (control of active power), as illustrated in Fig. 5a and 5b respectively.

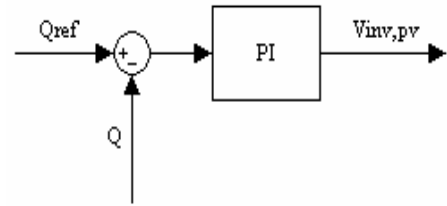


Fig. 5a. Reactive Power Control for the PV Array Inverter

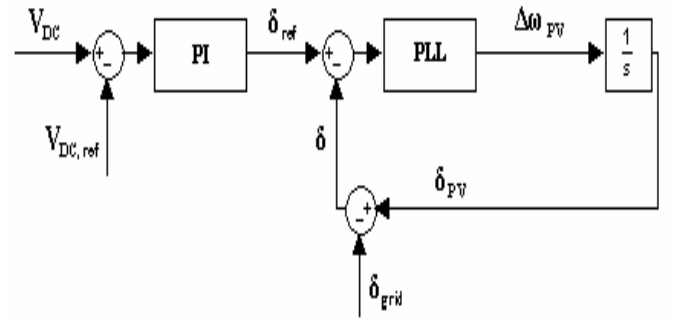


Fig. 5b. DC Voltage Control for the PV Array Inverter

The reactive power control is a feedback loop which continually monitors the error between the measured reactive power Q and its set point value Q_{ref} . The aforementioned error is used to adjust the inverter's terminal voltage so that the desired level of reactive power is maintained.

The DC voltage control loop consists of a conventional Phase Locked Loop (PLL), fed by a phase reference δ_{ref} which is produced by the monitored difference between the reference DC voltage $V_{DC,ref}$ and the actual DC voltage V_{DC} . Hence, the inverter's phase angle is adjusted in order to inject to the low voltage grid, the power produced by the PV array.

D. Battery Inverter Control Strategy

As an energy storage device, the battery should always provide the demanded power in order to keep the microgrid's frequency and voltage constant at their predetermined value (e.g. 50 Hz, 1 p.u.). The approach used in this paper, is the implementation of conventional f/U droops into the batteries inverters, thus downscaling the conventional grid control concept to the low voltage grid [1, 13]. By this way expensive

control bus systems are replaced by using the grid quantities voltage and frequency for the coordination of the components. For the adjustment of the frequency the output active power is measured and the output frequency is calculated according to the frequency droop.

The battery inverter power output is regulated according to the predetermined droop characteristics. Droop control consists of a frequency droop controller and a voltage droop controller, as shown in Fig. 6a and 6b respectively.

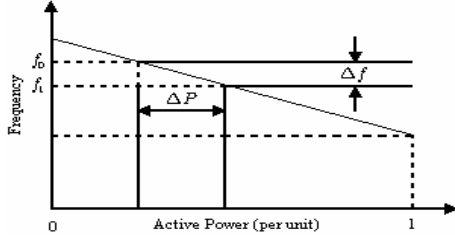


Fig. 6a. Typical frequency droop characteristic

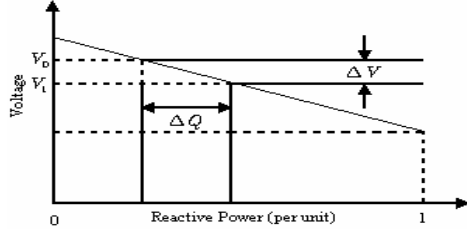


Fig. 6b. Typical voltage droop characteristic

Similarly to frequency control, the voltage control objective is to maintain output voltage close to nominal value.

E. Modeling of Loads

Electrical loads are assumed both as constant active and reactive power loads and constant R-L loads. The first assumption is modeled by the following dq-axis current components obtained from the absorbed active and reactive power:

$$I_d = \frac{V_d P}{V_d^2 + V_q^2} + \frac{V_q Q}{V_d^2 + V_q^2}, I_q = \frac{V_q P}{V_d^2 + V_q^2} - \frac{V_d Q}{V_d^2 + V_q^2} \quad (10)$$

Assuming that for the constant R-L load the load resistance R is connected in series with the load inductance L, then the voltage drop across the load V_L may be related to the load current I_L as:

$$V_L = R I_L + L \frac{dI_L}{dt} \quad (10)$$

III. SIMULATION RESULTS

The single line diagram of the microgrid system studied in this paper is illustrated in Fig. 1. The microsources considered comprise a photovoltaic generator equipped with a Maximum Power Point Tracker (MPPT) and a fixed speed wind turbine equipped with an induction generator. Different network configurations (e.g. ring configuration) have also been examined and it was shown that the proposed control strategies perform the same. A battery is used as energy

storage unit and is simply represented as a DC voltage source with adequate capacity, capable of meeting the real and reactive power commands within pre-specified limits. Wind speed and solar radiation vary randomly during simulation so that a large set of operating points is examined. For the illustrated results, base power of 100kW and base voltage of 380V, are used. Two constant admittance loads with $Y_1=0.25-j0.125$ p.u. and $Y_2=0.15-j0.0725$ p.u. have been considered. The parameters of frequency and voltage droop characteristics are $f_0=50$ Hz, $R_f=-0.02$, $V_0=1$ p.u., $R_v=0.05$.

During the first 70 seconds of the simulation microgrid is disconnected from the electrical grid. The next 70 seconds microgrid is connected to the electrical grid while during the last 70 seconds it is again disconnected.

Wind speed and solar radiation time-series are shown in figures 7 and 8, respectively. The produced powers by the wind turbine, the photovoltaic and the BES are shown in Figs 9, 10 and 11, respectively, where generator convention has been assumed. During the islanded mode of operation BES' control system continuously adjusts output active and reactive powers in order to keep the energy balance and also frequency and voltage close to their nominal values. However, when microgrid is connected to the grid output active and reactive powers are fixed to constant reference values, 0 p.u. and 0.35 p.u., respectively. Voltage profile at wind turbine and photovoltaic coupling nodes is shown in figure 12. BES' control system keeps the voltage close to 1 p.u., during islanding. Similarly, control system maintains frequency close to 50 Hz during islanded mode of operation. When microgrid is connected to the electrical grid, frequency is fixed at 50 Hz. The observed voltage and frequency deviations can be even smaller by changing the parameters of the voltage and frequency droop characteristics (Fig 6). In Fig. 14 the amplitude of the current flowing from to the grid is shown.

The transient oscillations of the voltage at wind turbine, photovoltaic coupling nodes and of the current flowing to the grid are shown in figures 15 and 16. Transient oscillations of 50 Hz occur during connection process and are being damped in about 0.5 sec. Control system's response during the transient phenomenon is stable and fast, ensuring stable transition to different modes of operation of the microgrid.

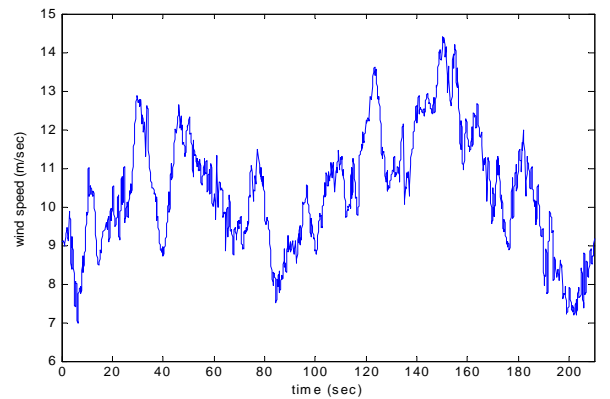


Fig. 7. Wind speed (m/sec)

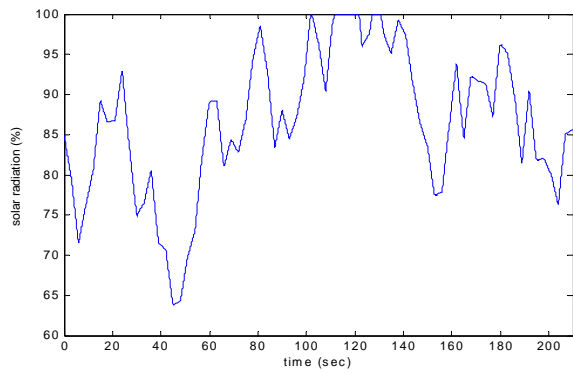


Fig. 8. Solar radiation (%)

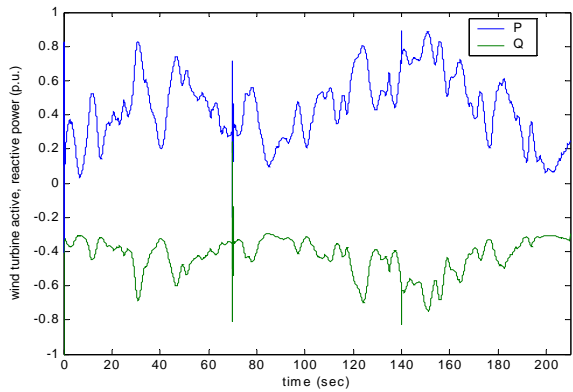


Fig. 9. Wind turbine's active, reactive powers (p.u.)

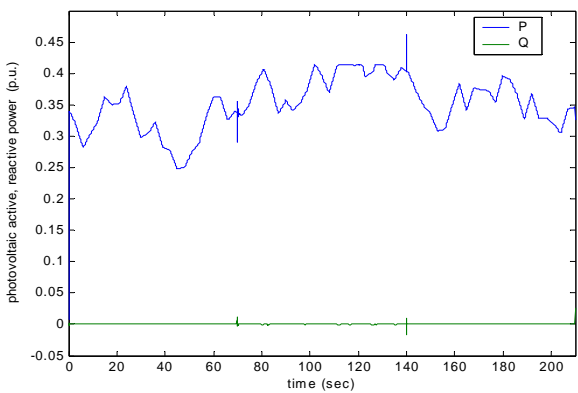


Fig. 10. Photovoltaic's active, reactive powers (p.u.)

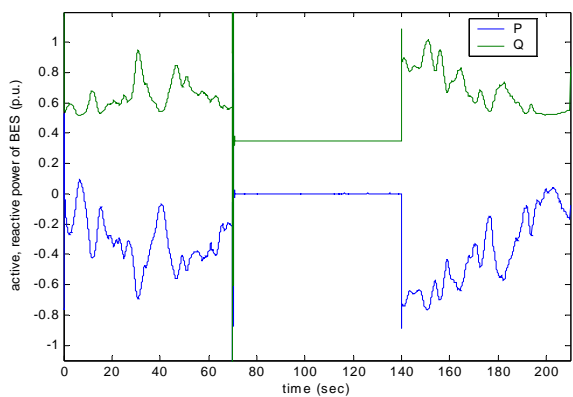


Fig. 11. Battery active, reactive powers (p.u.)

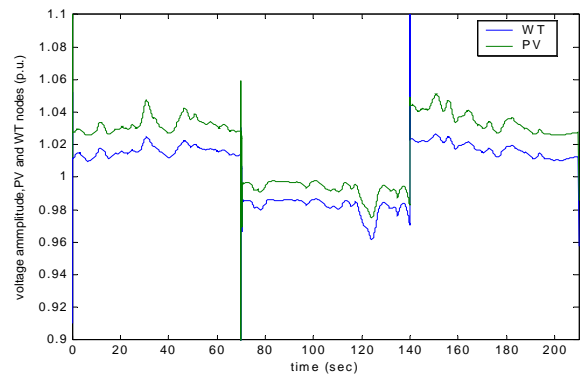


Fig. 12. Voltage amplitude at wind turbine, photovoltaic buses (p.u.)

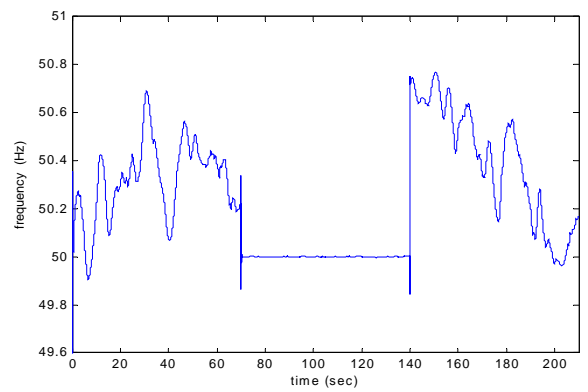


Fig. 13. Frequency measured at WT node (Hz)

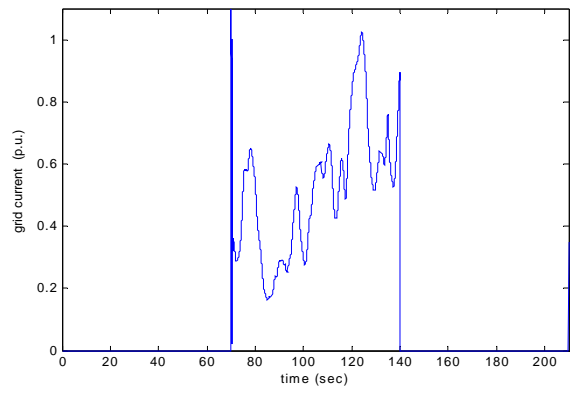


Fig. 14. Amplitude of current flowing to the grid (p.u.)

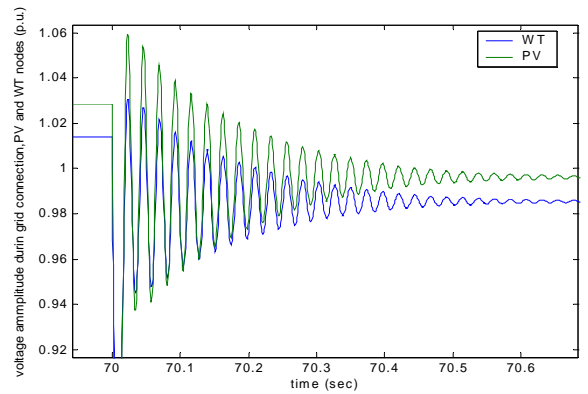


Fig. 15. Transients voltages of WT and photovoltaic coupling nodes during connection to the grid (p.u.)

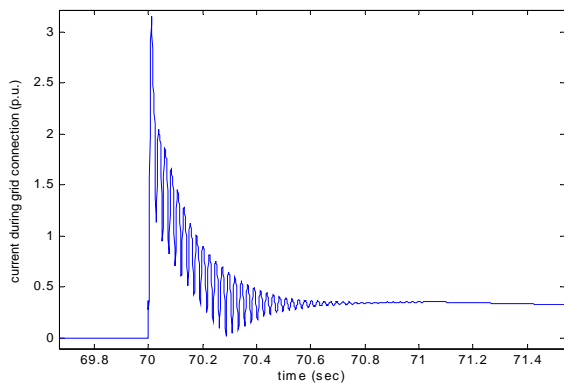


Fig. 16. Current transients during connection to grid (p.u.)

IV. CONCLUSIONS

In this paper, the operation of a typical microgrid is studied. The models of two dispersed generation units (wind turbine, photovoltaic system) are presented. Also models and strategies for fast control of microgrid frequency and voltage without communication are derived. The approach used in this paper, is the implementation of conventional f/U droops into the batteries inverters, thus downscaling the conventional grid control concept to the low voltage grid.

The aforementioned models are combined together and the model of a typical microgrid is simulated. The transients due to intentional islanding process are illustrated and it is proved that the proposed control scheme maintains frequency and voltage close to their nominal values for varying loads and climate conditions during islanded mode of operation. Furthermore, the stability of the microgrid is ensured during connection and disconnection to the grid.

V. ACKNOWLEDGMENT

The authors gratefully acknowledge all partners of the MICROGRIDS project (Contract ENK5-CT-2002-00610), especially of WPA, for their invaluable collaboration.

VI. APPENDIX

The parameters of the system depicted in Fig.1 are given next.

INVERTER CONTROL SYSTEM/DROOP PARAMETERS	
Frequency Controller	$f_o=1$ p.u., $R_f=-0.02$
Voltage Controller	$V_o=1$ p.u., $R_v=0.05$

WIND TURBINE	
$R=7.6$ m, $C_{p,max}=0.43$, $P_{nom}=90$ kW	
Induction Generator	
Stator resistance, r_s	0.0231 (p.u.)
Rotor resistance, r_r	0.0123 (p.u.)
Stator leakage Reactance, X_{ls}	0.1602 (p.u.)
Rotor leakage Reactance, X_{lr}	0.2632 (p.u.)
Magnetizing reactance, X_m	3.2013 (p.u.)

PHOTOVOLTAIC
$N_s=220$, $N_p=180$
$I_{tr} = 19.9693 \cdot 10^{-6}$ A, $T_r = 301.18$ °K, $K_i = 0.0017$ A/°C, $I_{scr} = 2.52$ A, $E_g = 1.12$ eV, $A = 1.92$, $K/q = 8.62 \cdot 10^{-5}$ eV/°K, $R_s=0.02$ Ω
MPPT
Voltage Controller – $K_v=0.01$, $I_v=0.05$

Base Quantities
$f_b=50$ Hz, $V_b=380$ V, $S_b=100$ kW

VII. REFERENCES

- [1] Engler A., "Applicability of Droops in Low Voltage Grids", International Journal of Distributed Energy Sources, Vol.1, number 1, pp 3-15, September 2004.
- [2] F. D. Kanellos, N. D. Hatziaargyriou, "The effect of variable speed wind turbines on the operation of weak distribution networks," *IEEE Trans. Energy Conversion*, vol. 17, pp.543-548, Dec. 2002.
- [3] Chee-Mun Ong, *Dynamic Simulation of Electric Machinery Using Matlab®/Simulink*, Prentice Hall PTR, New Jersey, 1998.
- [4] S. A. Papanthassiou, M. P. Papadopoulos, "Dynamic behavior of variable speed wind turbines under stochastic wind," *IEEE Trans. Energy Conversion*, vol. 14, pp. 1617-1623, Dec. 1999.
- [5] R. A. Messenger, J. Ventre, *Photovoltaic Systems Engineering* (2nd ed.), CRC Press, New York, 2004.
- [6] O. Wasynczuk, N. A. Anwah, "Modeling and dynamic performance of a self-commutated photovoltaic inverter system," *IEEE Trans. Energy Conversion*, vol. 4, pp. 322-328, Sep. 1989.
- [7] G. Vachtsevanos, K. Kalaitzakis, "A hybrid photovoltaic simulator for utility interactive studies," *IEEE Trans. Energy Conversion*, vol. EC-2, pp. 227-231, June 1987.
- [8] A.D. Hansen, P. Sørensen, L. H. Hansen and H. Bindner, "Models for a Stand-Alone PV System," Risø National Laboratory, Roskilde, Tech. Rep. Risø-R-1219 (EN)/SEC-R-12, Dec. 2000.
- [9] K. H. Hussein, I. Muta, T. Hoshino, M. Osakada, "Maximum photovoltaic power tracking: an algorithm for rapidly changing atmospheric conditions," *IEE Proc.-Gener. Transm. Distrib.*, vol. 142, pp.59-64, Jan. 1995.
- [10] C. Prapanavarat, M. Barnes and N. Jenkins, "Investigation of the performance of a photovoltaic ac module," *IEE Proc.-Gener. Transm. Distrib.*, vol. 149, pp. 472-478, July 2002.
- [11] M. R. Patel, *Wind and Solar Power Systems*, CRC Press, New York, 1999.
- [12] Siegfried Heier, *Grid Integration of Wind Energy Conversion Systems*, John Wiley & Sons Ltd, West Sussex, 1998.
- [13] M. C. Chandorkar, D. M. Divan and R. Adapa, "Control of parallel connected inverters in standalone ac supply systems," *IEEE Trans. Industry Applications*, vol. 29, pp. 136-143, Jan.-Feb. 1993.

VIII. BIOGRAPHIES

F. D. Kanellos graduated from the Department of Electrical and Computer Engineering of NTUA in 1998. He received the Doctor of Engineering degree in 2003. His research interests include modeling and control of wind turbines, modeling-system identification of networks with embedded wind parks, power electronics and neural networks.

A. I. Tsouchnikas received his Electrical and Computer Engineering degree at National Technical University of Athens (NTUA), in 2004. He is PhD student in the Electrical Engineering Department of NTUA. His research interests include renewable energy sources and dispersed generation.

N. D. Hatziaargyriou is Professor at Power Division of the Electrical and Computer Engineering Department of NTUA. His research interests include renewable energy sources, dispersed generation, dynamic security and AI techniques. He is member of CIGRE SCC6 and senior member of IEEE.